Journal of Colloid and Interface Science 415 (2014) 89–94

Contents lists available at ScienceDirect

Journal of Colloid and Interface Science

www.elsevier.com/locate/jcis

Synthesis and photocatalytic properties of bismuth titanate with different structures via oxidant peroxo method (OPM)

André E. Nogueira [a], Elson Longo [b], Edson R. Leite [a], Emerson R. Camargo [a,*]

[a] LIEC-Laboratório Interdisciplinar de Eletroquímica e Cerâmica, Departamento de Química, UFSCar-Universidade Federal de São Carlos, Rod.Washington Luis km 235, CP 676 São Carlos, SP 13565-905, Brazil
[b] Instituto de Química de Araraquara, UNESP-Universidade Estadual Paulista, Rua Francisco Degni, CP 355 Araraquara, SP 14801-907, Brazil

ARTICLE INFO

Article history:
Received 15 July 2013
Accepted 8 October 2013
Available online 22 October 2013

Keywords:
Bismuth titanate
Photocatalyst
OPM route

ABSTRACT

Bismuth titanate ($Bi_4Ti_3O_{12}$ and $Bi_{12}TiO_{20}$) powders were synthesized by the Oxidant Peroxide Method (OPM), and the effect of temperatures on physical and chemical properties of particles was investigated. The results showed that the morphology and average particle size of materials can be successfully controlled by adjusting the temperature. The samples after calcination were characterized by X-ray diffractometry, transmission electron microscopy, diffuse reflectance spectroscopy, Raman spectroscopy, and BET isotherms. The photocatalytic activity of materials was also evaluated by studying the degradation of 10 ppm aqueous rhodamine B dye under ultraviolet radiation.

1. Introduction

Currently, advanced oxidation processes (AOP) based on photocatalytic processes have been widely used as an alternative treatment of effluents, especially in the case of water contaminated by organic compounds. Although there are some peculiarities, the AOP mechanism for the degradation of contaminants is well known, as shown by Zhang et al. [1] for degradation of sulfadiazine using heterogeneous photocatalysis. However, new synthesis routes used to obtain improved materials for AOP, as well as studies about the inherent effects of synthesis strategies in the photocatalytic processes, have only been minimally explored.

Bismuth titanate, a large family that includes several phases in the Bi–Ti–O system, is a promising candidate for various technological applications, including effluent treatment [2]. The $Bi_4Ti_3O_{12}$ compound, which is generally used for applications such as memory storage, optical displays, piezoelectric converters and photocatalysis [3], has a layered perovskite structure built up by the regular intergrowth of $(Bi_2O_2)^{2+}$ layers and a perovskite type layer $(Bi_2Ti_3O_{10})^{2-}$, where Bi ions occupy the 12-coordinated sites [4]. Crystals of $Bi_{12}TiO_{20}$, on the other hand, belong to the sillenite family with crystal structures being formed by Bi–O polyhedra, where Bi ions are coordinated with five oxygens that form an octahedral arrangement with the Bi–O polyhedron network connected to regular TiO_4 tetrahedra [5].

In earlier studies, Yao et al. [6,7] showed that sillenite ($Bi_{12}TiO_{20}$) and perovskite ($Bi_4Ti_3O_{12}$) show high photocatalytic activity for organic dye degradation. Their photocatalytic activity can be attributed to the special electronic structure and the well dispersed electrons of Bi_{6S}, which can form the wide valence band and increase the mobility of electric charges. Bismuth titanates $Bi_{12}TiO_{20}$ and $Bi_4Ti_3O_{12}$ have different crystal and electronic structures, and may also possess band structures which can be increased in the quantum efficiency of the heterogeneous photocatalytic property by acting as electron (or hole) traps and by altering the e^-/h^+ pair recombination rate.

Several methods, including the solid state reaction [8], microemulsion method [3], co-precipitation [9], hydrothermal processing [10], mechanical synthesis [11] and sol–gel routes [12,13], have been developed for the synthesis of different phases of bismuth titanate powders. Yet, all of these methods have some drawbacks, including the appearance of secondary phases and the presence of non-stoichiometric compositions and undesired impurities [10].

A recent study, describing the oxidant peroxo method of synthesis (OPM), showed several promising advantages when compared to the other synthesis techniques, in terms of purity of the product, simple reactive conditions, and easier control of particle size; moreover this method is free from added contaminants such as chloride ions and organic compounds that could interfere in the properties and photocatalytic process [14–18].

* Corresponding author. Address: LIEC-Department of Chemistry, UFSCar-Federal University of São Carlos, Rod.Washington Luis km 235, CP 676 São Carlos, SP 13565-905, Brazil. Fax: +55 16 3351 8350.
E-mail addresses: andreesteves86@hotmail.com (A.E. Nogueira), elson@iq.unesp.br (E. Longo), edson.leite@pq.cnpq.br (E.R. Leite), camargo@ufscar.br (E.R. Camargo).

0021-9797/$ - see front matter © 2013 Elsevier Inc. All rights reserved.
http://dx.doi.org/10.1016/j.jcis.2013.10.010

The use of the OPM route to obtain reactive bismuth titanates for AOP can be particularly attractive, since impurities are avoided and crystalline materials can be formed at lower temperatures, excluding a series of interference usually present in different methods of synthesis. In this study, we report an easy method to prepare bismuth titanates ($Bi_4Ti_3O_{12}$ and $Bi_{12}TiO_{20}$) and the influence of the structure on the reaction of photocatalysis under UV radiation. This two-step preparation procedure consists of preparing an amorphous precipitate followed by a firing treatment. The amorphous precipitate was obtained at room temperature through the reaction between some aqueous soluble peroxo-complexes and bismuth ions. The photocatalytic activity of well crystalline bismuth titanates was tested on the degradation of rhodamine B (RhB) dye in aqueous solution, under UV-light irradiation.

2. Materials and methods

2.1. Synthesis

The amorphous precipitates with molar ratio Bi:Ti of 12:1 and 4:3 were synthesized as described by Camargo and Kakihana [15] through the dissolution of titanium metal powder (98% Aldrich, USA) in an aqueous solution of 60 mL of H_2O_2 (30%, analytical grade, Synth, Brazil) and 40 mL of aqueous ammonia solution (30%, analytical grade, Synth, Brazil). After approximately 3 h, a yellow transparent solution of peroxytitanate complexes was obtained. A second solution of Bi_2O_3 (99.99%, Aldrich, USA) was added into 10 mL of nitric acid (analytical grade, Synth, Brazil) and slowly added dropwise on the peroxytitanate solution under stirring and cooling in an ice-water bath. This resulted in vigorous gas evolution, forming an amorphous and yellow precipitate that was filtered and washed with diluted ammonia solution to eliminate all nitrate ions. The washed precipitate was dried at 60 °C for 3 h and ground and calcined at several temperatures between 400 and 900 °C for 1 h at a heating rate of 10 °C min^{-1} in closed alumina boats.

2.2. Characterization

All the powders (amorphous and heat-treated) were characterized at room temperature by X-ray diffraction (XRD) using Cu Kα radiation (Rigaku D/MAX 200, with a rotary anode operating at 150 kV and 40 mA) in the 2θ range from 10° to 75° with step scan of 0.02°. Raman spectra were obtained with a Horiba Jobin-Yvon Raman micro-spectrometer LabRAM at room temperature using the 633 nm line of a 5.9 mW He–Ne laser as the excitation source through an Olympus TM BX41 microscope. The Brunauer–Emmett–Teller (BET) isotherms were determined through nitrogen adsorption at 77 K (Micromeritics ASAP 2000). Diffuse reflectance spectra in the ultraviolet–visible region (DRS/UV–Vis) were recorded at room temperature in the 200–800 nm range using a Varian model Cary 5G in the diffuse reflectance mode (R) and transformed to a magnitude proportional to the extinction coefficient (K) through the Kubelka–Munk function [19]. From these spectra, the band gaps of the samples were determined according to the method proposed by Tauc [20]. The morphology of the powders was characterized by transmission electron microscopy (TEM) FEI/PHILIPS CM120.

2.3. Photocatalysis

Eighty milliliters of a 10 mg L^{-1} RhB dye solution at pH 6.0 was mixed with 60 mg of the catalyst and irradiated with ultraviolet light placed in a box at 25 °C, which was set at a distance of 30 cm from the beaker containing the catalyst and RhB dye. The radiation used in this experiment was obtained with a medium-pressure mercury vapor lamp (Osram, HQL 400) using output without a protection bulb to perform the photodegradation reactions. For the adsorption test, we used the same conditions except for the presence of UV radiation. All the tests were performed under vigorous stirring. Reactions were monitored by UV–Vis spectroscopy (JASCO V-660) at 554 nm, using a commercial quartz cuvette. The experiments were performed in quadruplicate.

3. Results and discussion

Generally, bismuth titanates are prepared by the solid-state reaction between Bi_2O_3 and TiO_2 at elevated temperatures; however, owing to some inherent limitations, this process yields large grain size and secondary phases [21,22]. In this study, pure $Bi_{12}TiO_{20}$ and $Bi_4Ti_3O_{12}$ powders were successfully prepared by the OPM route under mild crystallization conditions.

Hydrogen peroxide is a very attractive oxidant reagent for reactions in aqueous media and has been widely used in several procedures based on the "green chemical" approach [23]. In the OPM method, hydrogen peroxide is replaced by titanium peroxo-complexes synthesized *in situ* that act in a similar fashion toward H_2O_2 molecules. This reaction between soluble peroxo-complexes and bismuth ions results in the formation of a non-crystalline precipitate free of contaminants and without the generation of chemical waste. Particularly, a large amount of oxygen is released when this precipitate crystallizes, which increases the local oxygen pressure and strongly affects the final properties of the oxide formed [24]. It should be emphasized that these precipitates can be obtained at any desired Bi:Ti molar ratio, which means that the method can be highly tailored, allowing the synthesis of bismuth titanates with different structures and compositions.

Fig. 1a shows the XRD patterns of samples prepared with Bi:Ti molar ratio of 12:1 fired at different temperatures for 1 h. The absence of any diffraction peak in the XRD curve of the precipitate is of fundamental importance. Sometimes, wet-chemical routes form precipitates partially crystallized with undesired phases, resulting in stable secondary phases virtually impossible to be eliminated. Apart from the presence of a few small peaks of a secondary $Bi_4Ti_3O_{12}$ phase in the sample annealed at 400 °C (assigned with ●), all peaks in the samples heat-treated at 500 °C or higher were indexed on the basis of body-centered cubic (bcc) sillenite $Bi_{12}TiO_{20}$ (PDF 34-0097). In comparison with other methods of synthesis as disclosed by Ranieri et al. [25] and Thanabodeekij et al. [26], the OPM route requires a lower calcination temperature for obtaining pure phase.

X-ray diffraction patterns of the precipitate and calcined powders with Bi:Ti molar ratio of 4:3 are shown in Fig. 1b. The sample calcined at 900 °C for 1 h presented only the diffraction peaks corresponding to the $Bi_4Ti_3O_{12}$ phase (PDF 34-0097), without any trace of a secondary phase. However, samples annealed at lower temperatures showed the presence of the $Bi_4Ti_3O_{12}$ together with the sillenite ($Bi_{12}TiO_{20}$) as majority phase. It has been proposed that the synthesis of the $Bi_4Ti_3O_{12}$ by different routes occurs through the crystallization of sillenite $Bi_{12}TiO_{20}$ phase, before forming the perovskite $Bi_4Ti_3O_{12}$ [8,27]. It is interesting to note that the same sequence of reactions was observed here during the synthesis of $Bi_4Ti_3O_{12}$ by the OPM method, corroborating the idea that sillenite phase is always formed first at lower temperatures, and $Bi_4Ti_3O_{12}$ is only crystallized at higher temperatures, independent of the synthesis method.

Raman spectra of $Bi_{12}TiO_{20}$ samples calcined at 500–700 °C were all similar, confirming the high phase purity of the samples. Obviously, these spectra are quite different from those of the sample calcined at 400 °C (Fig. 2a) due to the presence of the secondary

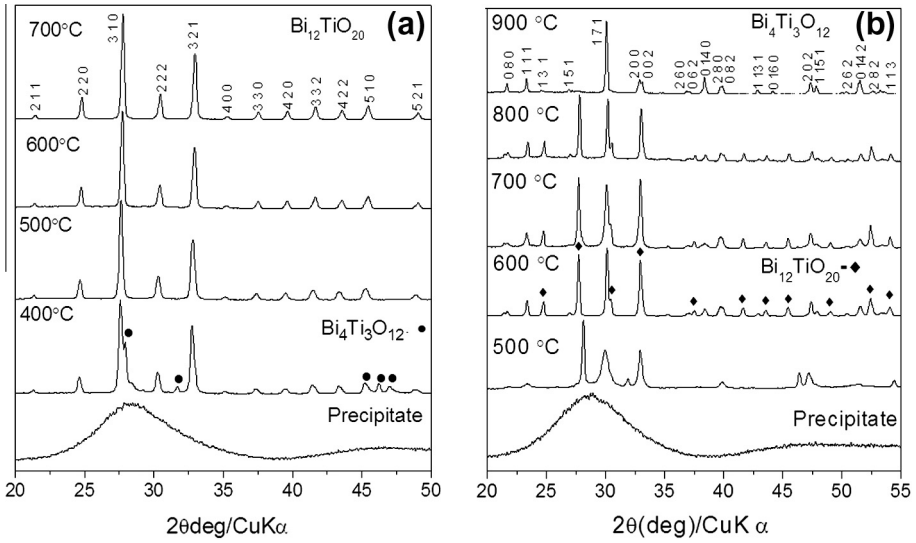

Fig. 1. X-ray diffraction patterns of $Bi_{12}TiO_{20}$ (a) and $Bi_4Ti_3O_{12}$ (b) calcined at different temperatures for 1 h.

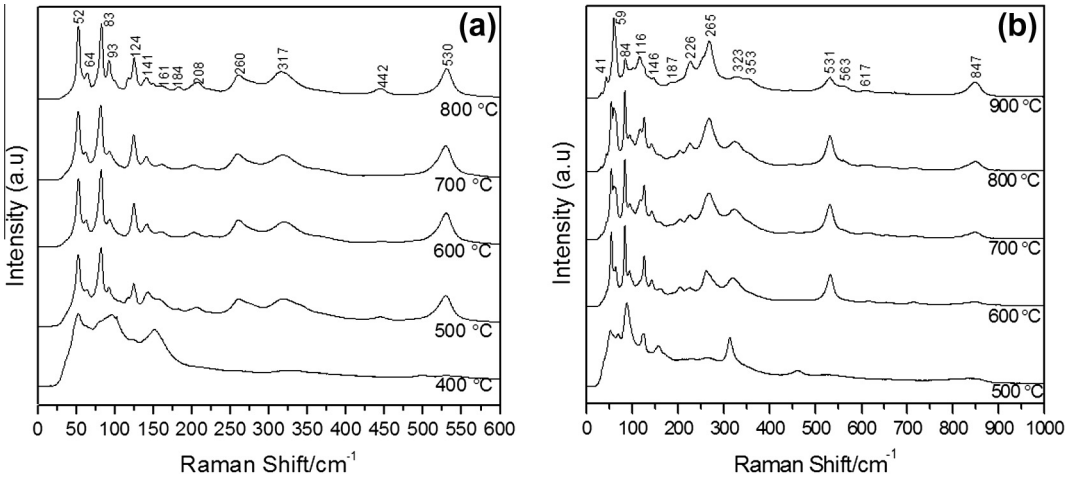

Fig. 2. Raman spectroscopy of $Bi_{12}TiO_{20}$ (a) and $Bi_4Ti_3O_{12}$ (b) calcined at different temperatures for 1 h.

phase. The bands in the range 208–530 cm^{-1} of the Raman spectra of pure $Bi_{12}TiO_{20}$ were attributed to the Bi–O bond vibrations, whereas the weak band at 720 cm^{-1} was assigned to the symmetric stretching of Ti–O tetrahedral [28].

The Raman spectra of $Bi_4Ti_3O_{12}$ are shown in Fig. 2b. It can be observed that the sample calcined at 900 °C exhibited all modes corresponding to $Bi_4Ti_3O_{12}$ orthorhombic structure, in good agreement with the XRD data. The Raman modes at 265, 323, 531, 617 and 847 cm^{-1} correspond to the internal vibration of the TiO_6 octahedra. The combination of the splitting modes at 265 and 226 cm^{-1} corresponds to a weak bending vibration of O–Ti–O in the TiO_6 octahedra [29]. The Raman modes with lower wavenumbers, such as the modes at 116 cm^{-1}, originated from the vibrations between Bi and O atoms.

The TEM micrographs of precipitate and calcined powders of both compositions are shown in Fig. 3. Images of the amorphous precipitates show highly agglomerated nanoparticles with irregular shape together with well-defined spherical Bi_2O_3 particles. The presence of these spherical particles is more evident due to the density contrast effect in the image of $Bi_{12}TiO_{20}$ precursor richer in bismuth, which can explain the reason for secondary phase formations at lower temperatures in this sample. Powders calcined at 500, 700 and 900 °C, on the other hand, did not present significant differences among microstructures. The image of heat-treated samples at 500 °C shows the presence of large secondary particles of complex shape formed from the partial sintering of smaller primary particles. This effect becomes much more pronounced in the samples fired at 700 and 900 °C. Pinto et al. [17] reported that one of the most outstanding features of the OPM powders are their reactivity, which can be verified by the partial sintering and presence of necks between particles.

It is well known that, in addition to the morphology and crystal structure, the optical property of photocatalyst also plays an important role in its photocatalytic activity. The optical properties of materials were examined using UV–Vis diffuse reflectance spectroscopy, which provides information about the electronic transition and band gap (Table 1). The spectra of the materials exhibit an absorption band ranging from 2.06 to 3.67 eV. It indicates that the $Bi_{12}TiO_{20}$ and $Bi_4Ti_3O_{12}$ nanocrystals prepared in the present study have a good photocatalytic potential, not only in the ultraviolet, but also in the visible light region. A redshift of the absorption edge toward the longest wavelengths of the $Bi_{12}TiO_{20}$ spectra (Fig. 4a) was observed with increasing calcination temperatures, and consequently, a decrease in the band gap energy. Spectra of

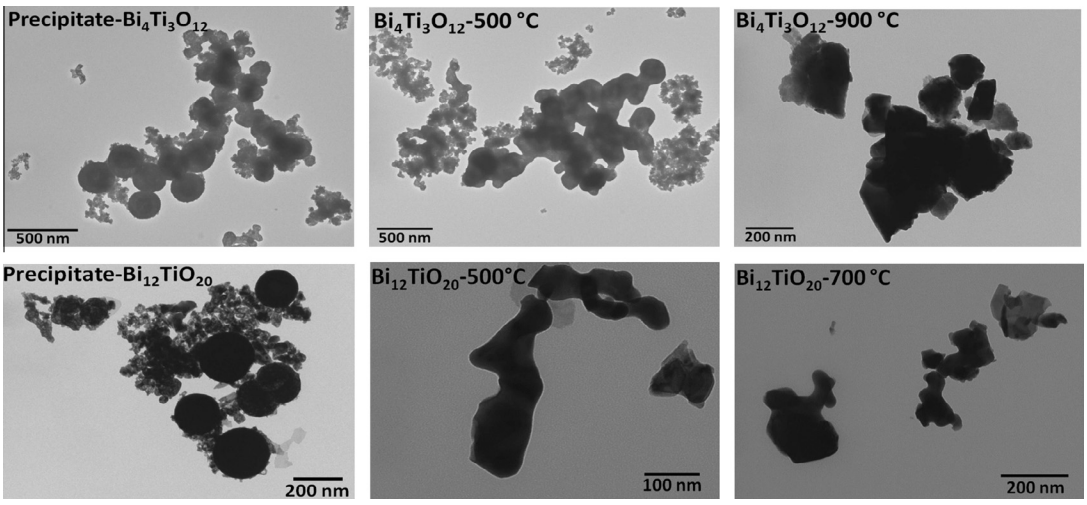

Fig. 3. Transmission electron microscopy image of the precipitate powder calcined at 500 °C, 700 °C and 900 °C for 1 h.

Table 1
Band gap energies.

Sample	Band gap/eV	
	$Bi_{12}TiO_{20}$	$Bi_4Ti_3O_{12}$
400 °C	2.66	–
500 °C	2.53	2.10 and 2.67
600 °C	2.57	2.06 and 2.64
700 °C	2.53	2.68
800 °C	–	2.65
900 °C	–	2.63

$Bi_4Ti_3O_{12}$ powders calcined at 500 and 600 °C (Fig. 4b) showed two absorption edges, which may be related to the presence of secondary phases identified by XRD and Raman characterization [30]. The spectra show a significant effect of calcination temperature on the optical characteristics of bismuth titanate of both compositions.

Titanium dioxide, on the other hand, is widely used in heterogeneous photocatalysis to degrade a broad range of pollutants due to its wide band gap of 3.2 eV that overlaps with sunlight emission [31]. However, $Bi_{12}TiO_{20}$ and $Bi_4Ti_3O_{12}$ samples synthesized by OPM absorb at wavelengths higher than TiO_2, which can constitute an advantage considering sunlight harnessing.

The photo-oxidation process of textile dye molecules is complex, but it is known that a photocatalytic reaction occurs generating some free radicals; for instance, OH., HO_2. and O_2^{-}., are generated and are responsible for the degradation of the dye and solution discoloration [32]. To evaluate the efficiency of the bismuth titanates synthesized by the OPM route, they were used to photodegrade RhB under UV radiation (Fig. 5). This dye has been used as a model compound in oxidation reactions for presenting strong absorption in the visible area (λ_{max} = 554 nm). It is high soluble in water and has properties similar to those presented by the textile dyes, which are difficult to degrade. In the absence of photocatalysts, the concentration of RhB decreased negligibly over the time, as can be seen in the curves labeled as without catalyst. We also investigated the decolorization process in the sample presence but in the dark, which was not shown in this publication. In this condition, the decolorization efficiency falls quite a bit and the corresponding data was about 5% for all materials. Obviously, the decolorization was not dominated by adsorption, but by photocatalytic degradation.

Linearized kinetic data curves for RhB photocatalytic degradation with samples are presented in Fig. 6. In aqueous dye solution, the photocatalytic decomposition reaction obeys first-order kinetics and the photocatalytic reaction can be simply described by $d[C]/dt = k[C]$, where [C] is the concentration of RhB, and k denotes the overall degradation rate constant [18]. The photocatalytic activity has been defined as the overall degradation rate constant of the catalysts. By plotting ln(C/Co) as a function of time through regression, we obtained the k (min^{-1}) constant from the slopes of the simulated straight lines for each sample (Table 2). Basically, the photocatalytic performance of a material is closely related to

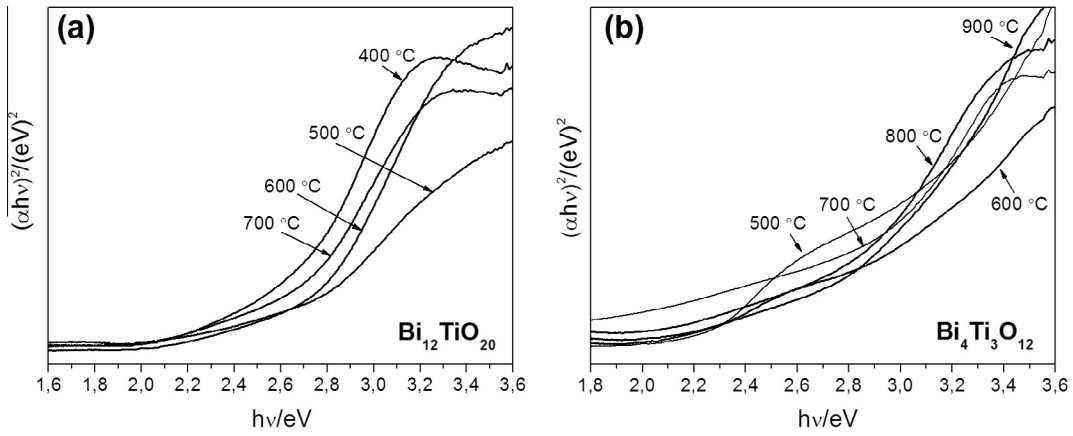

Fig. 4. UV–vis spectra of samples calcined at different temperatures for 1 h.

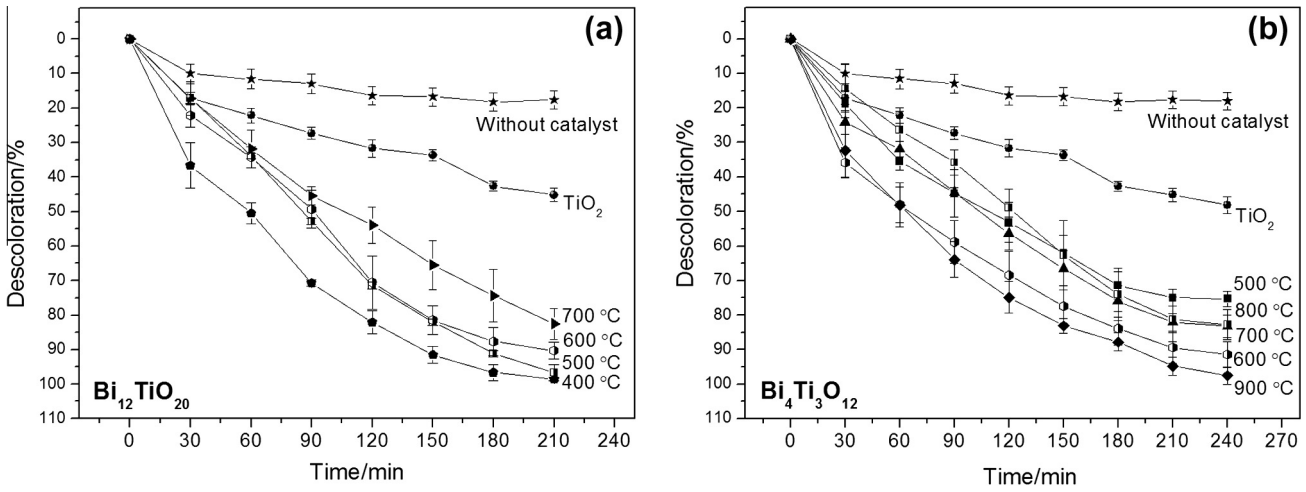

Fig. 5. The RhB normalization concentration in the solution (80 mL) with various catalysts versus the exposure time under UV-light irradiation.

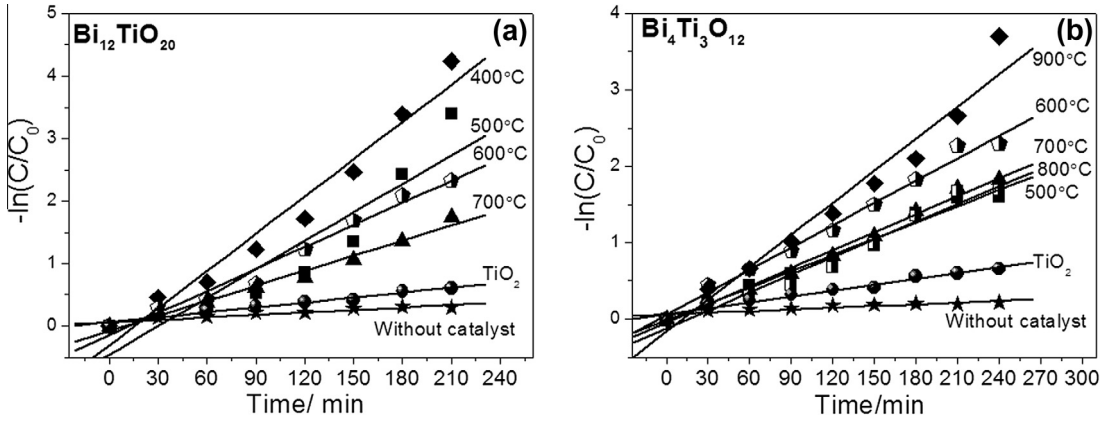

Fig. 6. First-order kinetics for the samples.

Table 2
The photocatalytic reaction rate constants, BET surface areas and the standard deviations of materials calcined at different temperatures for 1 h.

Sample	$k \times 10^{-3}$ (min^{-1})	R^2	Area m^2/g	Standard deviation (m^2/g)
Without catalyst	1.33	0.9016	–	–
TiO_2	2.61	0.9809	46.2	0.27
$Bi_4Ti_3O_{12}$-500 °C	7.10	0.9904	5.82	0.34
$Bi_4Ti_3O_{12}$-600 °C	9.70	0.9944	5.37	0.05
$Bi_4Ti_3O_{12}$-700 °C	7.90	0.9945	5.46	0.23
$Bi_4Ti_3O_{12}$-800 °C	7.80	0.9859	2.63	0.08
$Bi_4Ti_3O_{12}$-900 °C	14.00	0.9805	1.76	0.91
$Bi_{12}TiO_{20}$-400 °C	19.90	0.9823	6.62	0.02
$Bi_{12}TiO_{20}$-500 °C	15.20	0.9306	5.45	0.35
$Bi_{12}TiO_{20}$-600 °C	11.80	0.9886	4.46	0.03
$Bi_{12}TiO_{20}$-700 °C	8.10	0.9913	2.49	0.03

its characteristics of crystallinity, structure, surface area and band gap energy, among others.

During the reaction process, the band gap energy played an important role in determining the photoability of a catalyst. The relatively low band gap allowed the photo-absorption to increase and produce more electron (e^-) and hole (h^+) pairs, thus promoting the photocatalytic activities. In this study, the band gap energies of bismuth titanate synthesized catalysts were close, but lower than those of TiO_2 (3.0 eV), which may explain their relatively higher photocatalytic abilities.

In terms of textural analysis, the specific surface area was calculated by the BET equation. The results showed that an increase in calcination temperature caused a reduction in the specific surface area after thermal treatment. However, all materials presented low specific surface area and no significant influence on the photocatalytic activity of the materials.

4. Conclusions

The bismuth titanate powder was successfully synthesized by OPM method with different Bi:Ti molar ratios. The calcination temperature of 500 °C and time of 1 h was found to be sufficient to produce sillenite ($Bi_{12}TiO_{20}$) phase powder. The good photocatalytic

activity observed for material calcined at $Bi_{12}TiO_{20}$-400 °C and $Bi_{12}TiO_{20}$-500 °C was confirmed by the complete degradation of a 10 mg L^{-1} RhB solution within 3 h using ultraviolet light irradiation. The heating temperature has a significant influence on the crystalline phase and photocatalytic activity. This may be due to the heat-induced aggregation and reduction in defects. The formation of perovskite phase ($Bi_4Ti_3O_{12}$) occurs at 500 °C. However at 900 °C we observed only reflections corresponding to the $B_{i4}Ti_3O_{12}$ crystalline phase. The $Bi_4Ti_3O_{12}$-900 °C catalyst showed the best photocatalytic activity, achieving 98% solution discoloration.

Acknowledgments

This work was supported by the FAPESP (São Paulo Research Foundation, Grant No. 2010/20129-0, 2012/07067-0), CNPq and CAPES. We also acknowledge the INCTMN/CMDMF.

References

[1] J. Zhang, D. Fu, H. Gao, L. Deng, Appl. Surf. Sci. 258 (2011) 1294–1299.
[2] J. Hou, S. Jiao, H. Zhu, R.V. Kumar, J. Nanopart. Res. 13 (2011) 5557–5564.
[3] L. Xie, J. Ma, Z. Zhao, H. Tian, J. Zhou, Y. Wang, J. Tao, X. Zhu, Colloid Surf. A 280 (2006) 232–236.
[4] Z.Z. Lazarevic, N.Z. Romcevic, J.D. Bobic, M.J. Romcevic, Z. Dohcevic-Mitrovic, B.D. Stojanovic, J. Alloys Compd. 486 (2009) 848–852.
[5] X. Zhu, J. Zhang, F. Chen, Appl. Catal. B-Environ. 102 (2011) 316–322.
[6] W.F. Yao, X.H. Xu, J.T. Zhou, X.N. Yang, Y. Zhang, S.X. Shang, B.B. Huang, Appl. Catal. B-Environ. 52 (2004) 109–116.
[7] W.F. Yao, H. Wang, X.H. Xua, X.F. Chenga, J. Huangb, S.X. Shang, X.N. Yanga, M. Wang, Appl. Catal. A-General 243 (2003) 185–190.
[8] M.G. Navarro-Rojero, J.J. Romero, F. Rubio-Marcos, J.F. Fernandez, Ceram. Int. 36 (2010) 1319–1325.
[9] Y. Kan, P. Wang, Y. Li, Y. Cheng, D. Yan, Mater. Lett. 56 (2002) 910–914.
[10] D. Chen, X. Jiao, Mater. Res. Bull. 36 (2001) 355–363.
[11] R.A. Golda, A. Marikani, D.P. Padiyan, Ceram. Int. 37 (2011) 3731–3735.
[12] A.V.P. Rao, A.I. Robin, S. Komarneni, Mater. Lett. 28 (1996) 469–473.
[13] N.V. Giridharan, S. Madeswaran, R. Jayavel, J. Cryst. Growth 237–239 (2002) 468–472.
[14] E.R. Camargo, J. Frantti, M. Kakihana, J. Mater. Chem. 11 (2001) 1875–1879.
[15] E.R. Camargo, M. Kakihana, Chem. Mater. 13 (2001) 1181–1184.
[16] E.R. Camargo, M. Kakihana, J. Am. Ceram. Soc. 85 (2002) 2107–2109.
[17] A.H. Pinto, F.L. Souza, E. Longo, E.R. Leite, E.R. Camargo, Mater. Chem. Phys. 130 (2011) 259–263.
[18] V.R. Mendonça, C. Ribeiro, Appl. Catal. B-Environ. 105 (2011) 298–305.
[19] P. Kubelka, F. Munk, Tech. Phys. 12 (1931) 593–601.
[20] G.P. Joshi, N.S. Saxena, R. Mangal, A. Mishra, T.P. Sharma, Bull. Mater. Sci. 26 (2003) 387–389.
[21] A. Watcharapasorn, P. Siriprapa, S. Jiansirisomboon, J. Eur. Ceram. Soc. 30 (2010) 87–93.
[22] S. Kojima, A. Hushur, F. Jiang, S. Hamazaki, M. Takashige, M. Jang, S. Shimada, J. Non-Cryst. Solids 293–295 (2001) 250–254.
[23] R. Noyori, M. Aokib, K. Satoc, Chem. Commun. (2003) 1977–1986.
[24] E.R. Camargo, E. Longo, E.R. Leite, V.R. Mastelaro, J. Sol. State 177 (2004) 1994–2001.
[25] M.G.A. Ranieri, E.C. Aguiar, M. Cilense, A.Z. Simões, J.A. Varela, Ceram. Int. (2013) (In press).
[26] N. Thanabodeekij, E. Gulari, S. Wongkasemjit, Powder Technol. 160 (2005) 203–208.
[27] J.G. Lisoni, P. Millán, E. Vila, J.L. Martín de Vidales, T. Hoffmann, A. Castro, Chem. Mater. 13 (2001) 2084–2091.
[28] B. Mihailova, G. Bogachev, V. Marinova, L. Konstantinov, J. Phys. Chem. Solids 60 (1999) 1829–1834.
[29] Y.L. Du, G. Chen, M.S. Zhang, Solid State Commun. 132 (2004) 175–179.
[30] D. Li, H. Haneda, J. Photoch, Photobiol. A 155 (2003) 171–178.
[31] A. Esteves, L.C.A. Oliveira, T.C. Ramalho, M. Goncalves, A.S. Anastacio, H.W.P. Carvalho, Catal. Commun. 10 (2008) 330–332.
[32] S. Ma, R. Li, C. Lv, X. Wei, X. Gou, J. Hazard. Mater. 192 (2011) 730–740.